JOURNAL OF MATERIALS SCIENCE 31 (1996) 1005–1011

Transverse compressive testing of T300/914

A. LOWE*
Department of Materials Science, University of Cambridge, Pembroke Street, Cambridge CB2 3QZ, UK

The transverse compressive behaviour of a structurally complex carbon–epoxy unidirectional composite (T300/914) has been investigated over various temperatures and test rates. The mechanical behaviour was found to mirror the transverse tensile behaviour of the material, with the viscoelastic response being different between micro- and macroproperties. Composite macrofracture was found to occur at $\pm 34^\circ$ to the loading axis and was regular, whereas fracture of the bulk resin was irregular and occurred by Poisson forces, rather than compressive forces. The performance of the test fixture was assessed and found to be adequate for composites testing. An optimum specimen gauge length was determined as the ASTM recommendation was found to be unsatisfactory.

1. Introduction

The increasing importance of carbon fibre composites in major structural applications, such as the new Boeing 777 empennage [1], has meant that an improved understanding of the failure mechanisms in these materials under increasingly complex loading conditions needs to be achieved.

Unidirectional carbon fibre reinforced plastic (CFRP) is rarely used in structural components as they are usually manufactured from multidirectional laminates, several plies thick. The lay-up of the material is chosen to optimise the properties of the structure. The basic structural units are, however, individual plies of unidirectional CFRP. Therefore, if accurate property predictions are required, a knowledge of individual ply properties is essential. The properties of a single ply are difficult to produce accurately. Therefore, prediction of properties from multi-ply unidirectional laminates is used.

Of all mechanical properties, the least documented is transverse compressive behaviour. It has not been regarded as being important in structural design and therefore little published data is available. However, transverse compression is a shear process and is therefore likely to occur in some form in most structures. Accurate transverse compressive results are very difficult to obtain as highly erroneous results will ensue if specimen buckling is not suppressed or if the specimens are not perfectly aligned within the test fixture. If the specimen is constrained along its gauge length, account must be taken as to how the loading configuration is changed. Many tests rely on shear load transfer as a means of applying a compressive load, and this is known to cause a problem with stress concentrations at the ends of the specimen.

Specimen buckling will occur if the specimen gauge length is too long; but if it is too short, then the state of pure compressive stress within the specimen may be affected by the shear loading mechanisms and by end effects due to tabbing. Also, transverse compressive failure may not be catastrophic, but a gradual process involving buckling of the specimen, deformation of the matrix followed by a progressive crush. Therefore, definition of the true failure stress value can be ambiguous.

2. Experimental procedure

2.1. Transverse compressive test fixture

There are a multitude of longitudinal and cross-ply compressive test methods in existence [2–16], thus it was necessary to choose a particular method and modify it for a transverse testing program. The celanese compressive fixture [2–5, 16] was chosen as it is a recognised standard [3] and is proven for 0° and cross-ply strength and modulus measurements. It proved easy to manufacture, durable, highly compatible with the test frame and quickly equilibrated under varying thermal conditions.

2.2. Test materials

T300/914 is a commercially available carbon fibre–epoxy prepreg system consisting of carbon fibres embedded within a blend of two glycidyl amine epoxy resins (GY720 and ERL0510) modified with a small amount of (polyethersulphone) (PES) and hardened

* *Present address*: Faculty of Engineering and Information Technology, Department of Engineering, The Australian National University, Canberra ACT 0200, Australia.

0022–2461

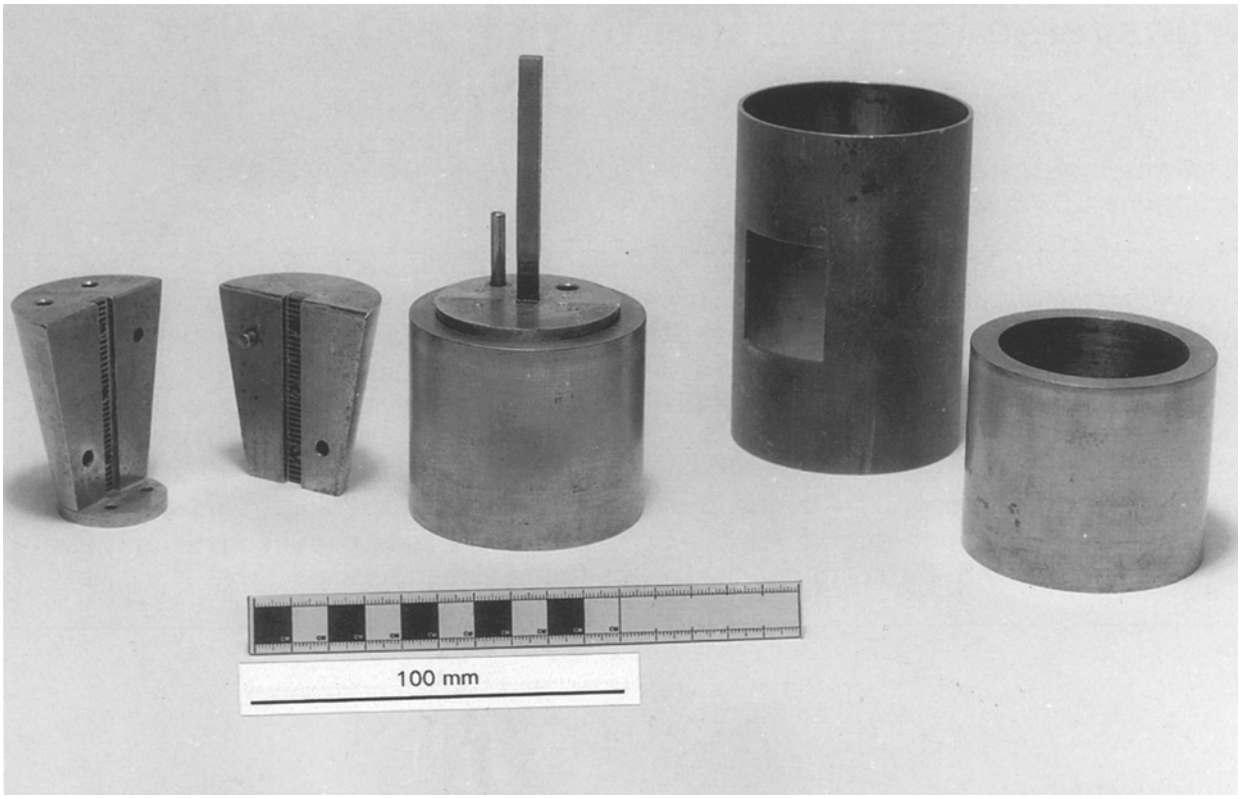

Figure 1 Partially assembled Celanese compressive test fixture with specimen.

with dicyanodiamide and/or diaminodiphenylsulphone. This material, when cured, is structurally very complex [17–20] consisting of carbon fibres embedded within a two phase resin consisting of epoxy based particles, approximately 1 μm in diameter surrounded by a poly(ethersulphone) (PES) based connecting matrix. Additionally, the fibres are coated in an epoxy-based interphase region, approximately 0.7 μm thick. The structure of the composite and bulk resin have been successfully modelled [20]. The composite prepreg was obtained from Ciba Geigy plc. Duxford, UK and processed into unidirectional laminates, 300 mm square and 24 plies thick, by Rolls Royce plc. Derby, UK [21]. Cured bulk resin was obtained from Ciba Geigy plc. Marly, Switzerland, in sheets, 200 mm square and 2 mm thick.

2.3. Measurements

The tests were performed at a test rate (R) of $10°\,mm\,min^{-1}$ over a temperature range of $-40°$–140 °C at 20 °C intervals, or at a temperature (T) of 23 °C over a test rate range of 10^{-2}–$10^{2}\,mm\,min^{-1}$ at 10^{1} intervals. Modulus, strength and fracture strain data were obtained from stress–strain plots, with fractographic and optical studies being used to determine the macro- and micromechanics of fracture and to assess the performance of the test specimens and fixtures.

The transverse compressive test specimens were based on ASTM dimensions [3] and were 6.7 mm wide, 140 mm long and 24 plies (3.3 mm) thick with 1 mm thick tabs at each end tapered at 30° towards the gauge length. Although aluminium tabs are recommended, glass/epoxy tabs were used, as under thermal variations, glass cloth tabs presented less of a thermal mismatch than aluminium. It became evident during testing that the ASTM recommended gauge length of 12.7 mm was too long, resulting in premature fracture, so a series of tests were performed using specimens of various gauge lengths to determine an optimum value. As the bulk resin specimens were only 2 mm thick, the specimen dimensions were reduced accordingly to keep the same gauge length-to-thickness ratio as the composite specimens. A typical composite test specimen and the partially assembled Celanese test fixture as shown in Fig. 1. An Instron 8032 servo-hydraulic test frame fitted with an environmental chamber was used for all testing.

3. Results and discussion

Fig. 2 shows the variation of transverse compressive strength (under standard conditions of T = 23 °C and $R = 10°\,mm\,min^{-1}$) with specimen gauge length. Below 8 mm, the strength was independent of gauge length, whereas above 8 mm, a rapid decrease in strength was observed, associated with premature buckling. Experimental scatter also increased markedly, indicating the random nature of the fracture process. For all subsequent fracture tests, a gauge length of 7 mm was chosen. Such a value gave consistent strength values and was sufficiently large to minimize edge effects at the tabs.

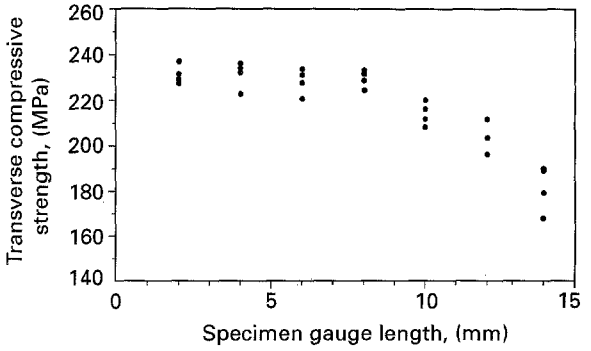

Figure 2 The variation of transverse compressive strength with specimen gauge length (temperature = 23 °C, test rate = 1 mm min^{-1}) for unidirectional T300/914.

The variation of transverse compressive strength, $\sigma_{\perp c}$, with temperature and test rate is shown in Figs 3 and 4 respectively. Experimental scatter was greater at the lower temperatures and the trends were linear as described by Equations (1) and (2).

$$\sigma_{\perp c} = 204.14 - 15.34\left(\frac{T}{T_0} - 1\right) \quad (1)$$

$$\sigma_{\perp c} = 244.49 + 11.51\left(\frac{R}{R_0} - 1\right) \quad (2)$$

Fig. 3 also shows bulk resin compressive data and from this it is obvious that the bulk resin strength is lower than the composite strength.

The variation of transverse compressive modulus, $E_{\perp c}$, with temperature and test rate is shown by Figs 5 and 6 respectively, and linear fits to the data were according to equations (3) and (4).

$$E_{\perp c} = 8.65 - 0.39\left(\frac{T}{T_0} - 1\right) \quad (3)$$

$$E_{\perp c} = 10.09 + 0.24\left(\frac{R}{R_0} - 1\right) \quad (4)$$

The variation of transverse compressive fracture strain, $\varepsilon_{\perp c}$, with temperature and test rate is shown in Figs 7 and 8 respectively with Equations (5) and (6) best describing the linear trends. The strain values (units = %) were substantially higher than the tensile strains reported in [20].

$$\varepsilon_{\perp c} = 3.02 + 0.16\left(\frac{T}{T_0} - 1\right) \quad (5)$$

$$\varepsilon_{\perp c} = 2.89 - 0.13\left(\frac{R}{R_0} - 1\right) \quad (6)$$

Fracture strain values were obtained from specimens of 7 mm gauge length.

Fig. 3 also shows the variation of compressive bulk resin strength with temperature, and includes the manufacturers' compressive strength data [22]. The resin strength was lower than the corresponding transverse composite strength. This is not usually the case and may be a result of the complex stress patterns associated with the composite [20]. The decrease in resin strength with temperature ($d\sigma/dT$) appeared to

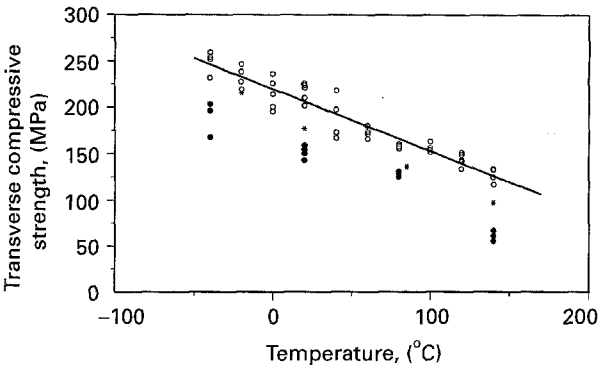

Figure 3 The variation of transverse compressive strength (○) with temperature (test rate = 10° mm min^{-1}) for unidirectional T300/914. Also shown are the bulk resin data obtained from this study (●) and from Ciba Geigy [22] (*).

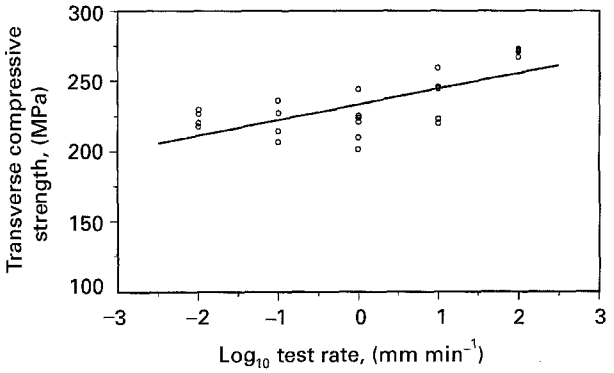

Figure 4 The variation of transverse compressive strength with test rate (temperature = 23 °C) for unidirectional T300/914.

match that experienced by the composite. However in Fig. 5, the resin modulus clearly possessed a different temperature response to the composite.

The stress–strain response of unidirectional T300/914 tested in transverse compression at temperatures of −40 °C, 23 °C and 140 °C (standard test rate) is shown in Fig. 9. Plastic deformation, especially at the higher temperatures, was extensive. However, the total strain-to-failure was low.

3.1. Viscoelastic characterization

The compressive data presented in this section mirrored the tensile data seen in [20], where a parameter was introduced, Λ, that characterized the viscoelastic response of the unidirectional composite over the specified temperature and test rate ranges. Λ is defined as the temperature change required at a standard test rate to attain a property variation caused by a unit test rate variation at a standard temperature and takes the units min °C mm^{-1}. A value of 17.2 was obtained for transverse compressive strength (i.e. the transverse compressive strength initially under standard conditions changes as much over a temperature range of 17.2 °C as it does over a test rate range of 10^1 mm min^{-1}), with values of 13.5 (transverse compressive modulus) and 17.5 (transverse compressive fracture strain) also obtained. When compared to the tensile values of 17.1 for strength, 13.8 for modulus

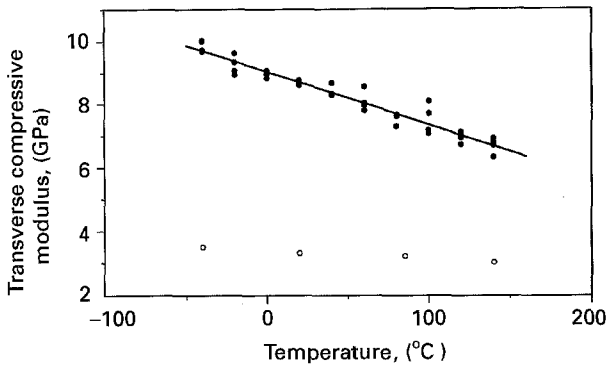

Figure 5 The variation of transverse compressive modulus (●) with temperature (test rate = 10° mm min^{-1}) for unidirectional T300/914. Also shown are the bulk resin data obtained from Ciba Geigy [22] (○).

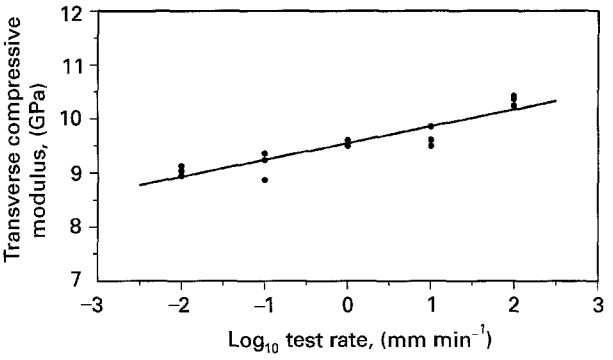

Figure 6 The variation of transverse compressive modulus with test rate (temperature = 23 °C) for unidirectional T300/914.

and 17.8 for fracture strain it is evident that the viscoelastic response of T300/914 is independent of loading mode. The well defined difference between macro- and microparameters observed in the Λ values is also seen in Figs 3 and 5 which show that the viscoelastic response of the composite is similar to the bulk resin in terms of strength, but not in terms of modulus.

3.2 Failure mechanisms

Fig. 10 (a transverse compressive fracture surface obtained under standard conditions at an area of high V_f) reveals the nature of the composite structure and clearly shows the multiphase nature of the material. Increased plastic deformation in the thermoplastic connecting phase under compressive loading and the presence of cusping in the interphase region are the only differences between the tensile and compressive fracture morphologies. This latter observation is not surprising as transverse compression is essentially a shear process. In areas of low V_f, the two phase resin also undergoes cusping, but this is very difficult to see fractographically as the resin structure tends to mask the cusped regions. The high level of bare fibre surface observed is caused by the interphase region being mutually shared by more than one fibre in areas of high fibre volume fraction and preferentially failing at the fibre/interphase interface rather than through the interphase region itself. In the lower half of Fig. 10, a fibre has been removed, exposing the

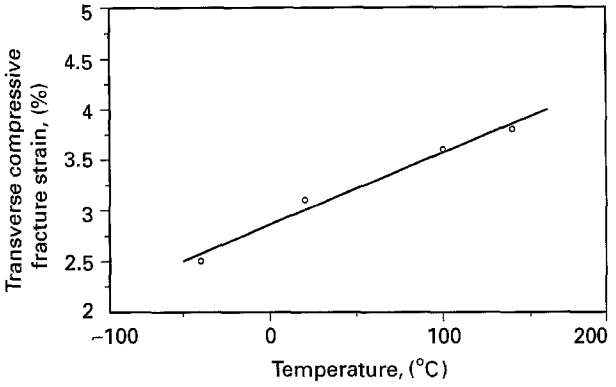

Figure 7 The variation of transverse compressive fracture strain with temperature (test rate = 10° mm min^{-1}) for unidirectional T300/914.

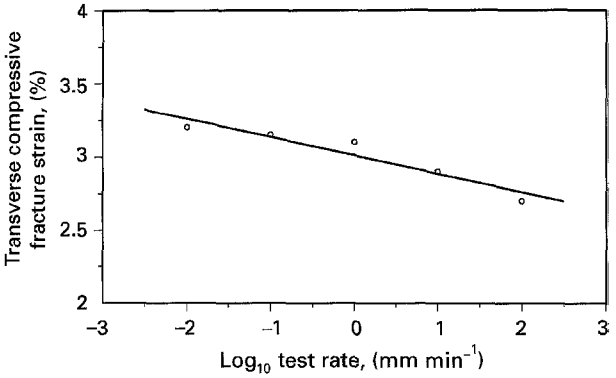

Figure 8 The variation of transverse compressive fracture strain with test rate (temperature = 23 °C) for unidirectional T300/914.

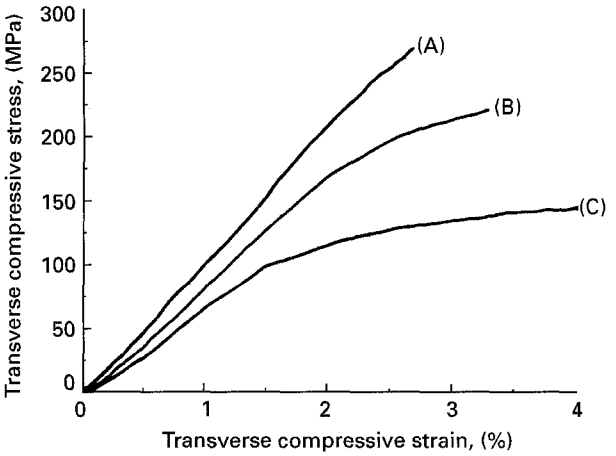

Figure 9 The stress/strain curves obtained for unidirectional T300/914 under transverse compressive loading obtained at 10° mm min^{-1} and at (A) −40 °C, (B) 23 °C and (C) 140 °C.

interphase/fibre interface and a distinct fracture morphology.

3.3 Macrofracture of the composite

Fracture of large gauge length specimens was premature and irregular due to the buckling forces exerted at increasing loads, as typically seen in Fig. 11. The buckling forces have caused one side of the specimen to detach in the gauge length region whilst causing

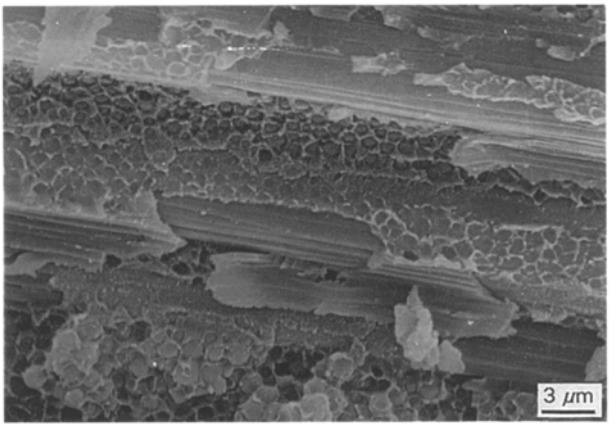

Figure 10 Unidirectional T300/914 transverse compressive fracture surface obtained at 10° mm min^{-1} and 23 °C showing large degree of interfacial failure seen in areas of high fibre volume fraction.

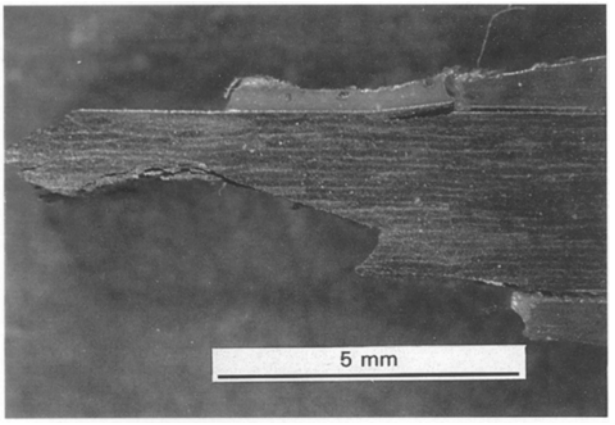

Figure 11 Typical premature compressive fracture by buckling (side view) of a T300/914 Celanese transverse compressive test specimen of gauge length 12.7 mm (temperature = 23 °C, test rate = 10° mm min^{-1}).

a relatively regular compressive-type fracture on the other. Fig. 12a–d schematically details this fracture mechanism. When the compressive load (a) reaches a critical point, buckling forces start to generate in the specimen gauge length (b). The point at which these forces appear depends on factors such as specimen alignment and quality. These forces act in one direction, resulting in one face being loaded in tension and one in compression (c). As the tensile strength of the material is lower than the compressive strength in transverse loading, tensile cracking initiates first and when coupled with any axial cracking (discussed later) result in instantaneous wholesale failure and fragmentation of the tensile face whereas the compressive loadings on the opposite face induce regular compressive failure (d). Fractographic examination (not presented in this work) confirmed these observations by revealing areas of both tensile and compressive fracture morphology.

Fracture of specimens possessing small gauge lengths was more regular. Fig. 13 shows a typical fracture profile. The fracture angle of approximately $\pm$ 34° to the specimen axis was not as expected (it is usually $\pm$ 45° for most materials). However, this value was constant throughout all the fracture tests and was

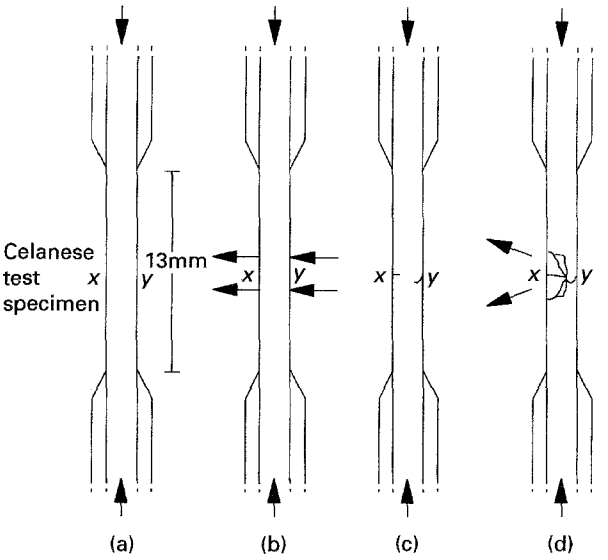

Figure 12 Macroscopic transverse compressive fracture mechanism for celanese specimens of gauge length 12.7 mm (a) Specimen under initial compressive load; (b) Buckling of the specimen in the centre section; (c) Tensile cracking on the tensile face of the specimen; (d) Premature fracture by buckling and fragmentation of the test section.

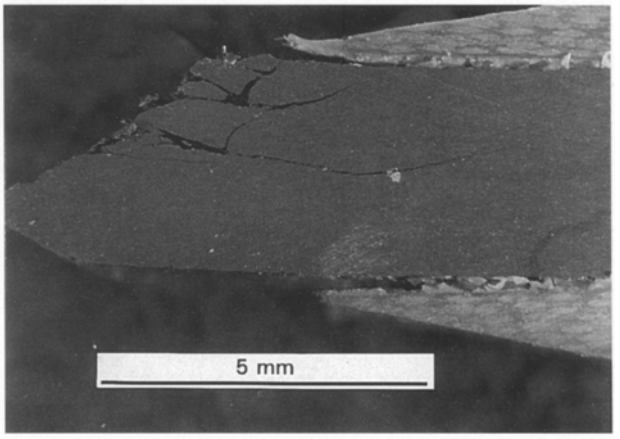

Figure 13 Typical transverse compressive fracture of a T300/914 Celanese test specimen of gauge length 7 mm showing axial cracking, tab debonding and a fracture angle of c.34° (temperature = 23°C, test rate = 10° mm min^{-1}).

in agreement with Mohr's strength criterion [23], which relates the interlaminar shear strength, τ_{12}, to $\sigma_{\perp c}$ in terms of compressive failure angle, as shown in Equation (7) and relies on the assumption that the compressive and shear stresses are at their most active at an angle, ϕ to the loading direction i.e.

$$\tan \phi = \frac{2\tau_{12}}{\sigma_{\perp c}} \quad (7)$$

At ambient temperature, τ_{12} = 72.6 MPa [24] and ϕ = 34°. This relationship has been found to be true at all test temperatures and macroscopic examination of the fracture profiles revealed that ϕ is independent of temperature. A similar expression has been developed by Skudra [23], which assumes that in the axial plane, the strengths are equivalent in all directions. This consequently results in an inaccurate estimation of ϕ, implying that this assumption is not valid for this

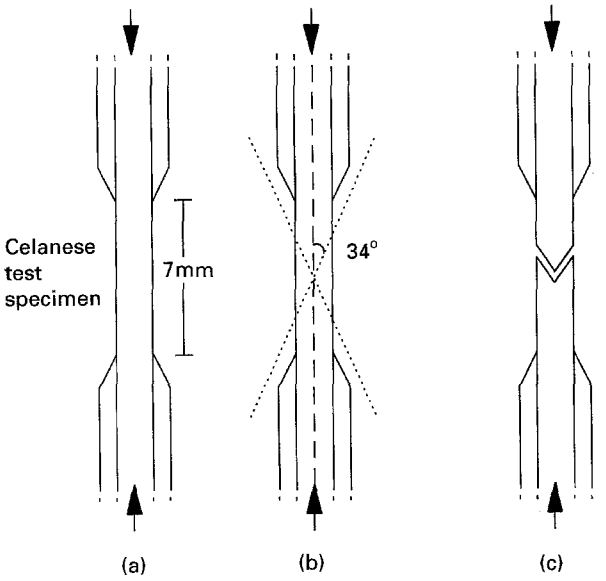

Figure 14 Macroscopic transverse compressive fracture mechanism for Celanese test specimens of gauge length 7 mm. (a) Specimen under initial compressive load. (b) Shearing along the maximum shear stress directions ($\pm$ 34°). (c) Fracture of the specimen at $\pm$ 34°, forming an angular/chevron fracture morphology.

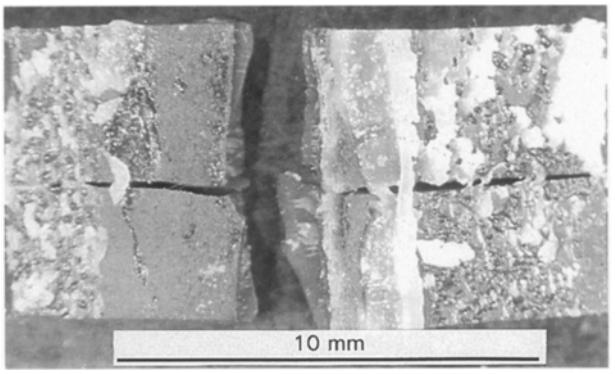

Figure 15 Typical compressive fracture of a bulk 914 resin Celanese test specimen of gauge length 4.3 mm, showing extensive axial cracking and regions of tab debonding.

particular test fixture, or test material. The value of $\pm$ 34° for the compressive failure angle was also in accordance with the structural models developed in [20] that revealed $\pm$ 34° to be the angle of maximum stressing in the two-phase resin when the composite experienced a transverse load. As the composite clearly fails in compression within the two phase resin structure, this agreement is not unexpected. The macro-fracture mechanism is shown schematically in Fig. 14a–c. On application of an increasing compressive load (a) shear stresses start to form along the maximum shear stress axes (b) resulting in fracture of the specimen along these lines forming an angular/chevron-type fracture profile (c). On many specimens, the vertex of the fracture surface was not located in the mid-plane of the specimen. This may have been caused by inaccurate specimen alignment relative to the fixture (i.e. irregular tabbing) or by inhomogeneities within the specimen resulting in fracture initiating at non-opposite points along the gauge length. The axial cracks seen in Fig. 13 were a common feature.

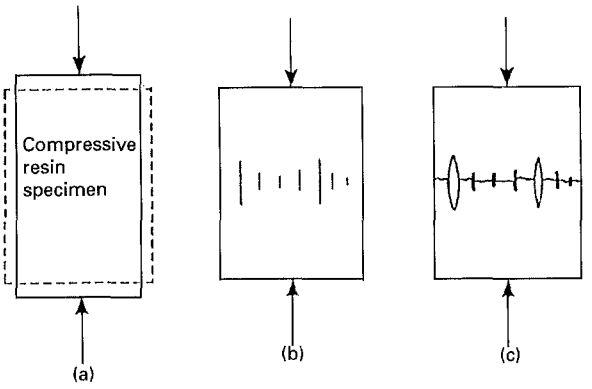

Figure 16 Macroscopic compressive fracture mechanism for bulk 914 resin celanese test specimens of gauge length 4.3 mm. (a) Poisson contraction under initial compressive load; (b) Formation of axial cracks; (c) Growth of axial cracks and eventual fracture of the specimen.

The cause of these cracks could be attributed to post-fracture crushing or Poisson contraction of the specimen.

Fig. 15 shows a typical bulk resin compressive fracture morphology. The area under view is the gauge length region. The areas of irregular morphology correspond to areas of tab debonding. Tab debonding due to thermal mismatch was a common problem for both composite and resin tests, although it did not appear to adversely affect the test data or occur under tensile loading. This detachment was also attributed to Poisson effects. It was evident that Poisson contraction had been a major factor in the compressive fracture of bulk resin specimens, as indicated by the presence of major axial cracking. This phenomenon would appear to be the result of specimen geometry. These axial cracks appeared to act as nucleation sites for transverse crack propagation, resulting in a surface morphology closer to tensile fracture than compressive fracture. Fig. 16a–c illustrates the fracture of bulk resin compressive specimens on a macro-level. The applied compressive load causes Poisson contraction of the specimen (a) which eventually exceeds the tensile fracture strain of the material, resulting in the formation of several axial splits (b). These splits multiply and grow until the section can no longer sustain the compressive load, and catastrophic failure occurs (c). This type of mechanism suggests that true compressive fracture of the material was not realised. At the higher temperatures, axial cracking was minimal. This was not surprising since the increased plastic deformation meant that the strain required to form these cracks was much higher than at low temperatures and exceeded that supplied by Poisson contraction.

3.4. Property modelling

The transverse compressive mechanical property trends observed followed those previously reported for transverse tensile testing, and so it would not be unreasonable to assume that the modified Halpin–Tsai model developed in [20] would apply to compressive behaviour. However, no compressive

fibre data were available and so the assumption that this model provides accurate transverse compressive predictive models is only a hypothesis.

The Tsai–Hahn strength equation [25] can be used to provide a curve fitted strength model for the composite under transverse compressive loading i.e.

$$\sigma_{\perp c} = \left(1 + V_f\left(\frac{1}{\Sigma} - 1\right)\sigma_r\right)K_T^{-1} \qquad (8)$$

where σ_r is the resin compressive strength [22], Σ is the stress partitioning factor and K_T is a stress concentration factor. By curve fitting, $\Sigma = 0.978$ and $K_T = 0.014$. As the presence of the interphase does not appear to influence the viscoelastic strength behaviour, the absence of interphase terms from Equation 8 is not critical.

4. Conclusions

The transverse compressive behaviour of unidirectional T300/914 has been established over various temperatures and test rates, with the bulk resin strength values lower than the composite strength values.

For transverse compressive testing of unidirectional specimens, the ASTM recommended aspect ratio was found to be unsuitable and an optimum aspect ratio has been determined.

Tab debonding due to thermal mismatch was a problem and so unidirectional carbon–epoxy tabs should be considered, rather than glass cloth–epoxy tabs.

True compressive failure seems only to have been partially achieved by using the celanese test fixture. Whereas the composite data were reliable, the resin test data were approximately 10% lower than those obtained by the manufacturer (using small compressively loaded cubes). This was attributed to axial cracking of the material when loaded and so a specimen geometry that minimizes Poisson expansion needs to be designed. Axial cracking reduces at high temperatures.

Transverse compressive microfracture of the material occurs by shearing of the thermoplastic-based connecting phase and particle/matrix debonding. Interphase/fibre debonding was more common than previously observed under tensile loading, implying that this interface is weaker in shear.

The compressive failure angle was found to be $\pm 34°$, in accordance with structural modelling of the system and with the Mohr strength criterion.

Acknowledgements

The author thanks Professor Derek Hull for the use of the facilities at the Department of Materials Science, University of Cambridge, and also the staff and colleagues who helped in this work both in Cambridge and overseas.

References

1. K.H. SCHREIBER, J.T. QUINLIVAN, Oral presentation at ICCM/9: Ninth International Conference on Composite Materials. Madrid July 1993.
2. I.K. PARK in Proceedings of the International Conference on Carbon Fibres, Components and Applications (The Plastics Institute, London, 1971) pp. 194–202.
3. D3410-75 ASTM Annual Book of Standards (American Society for Testing and Materials, Philadelphia, PA, 1985).
4. N.L. HANCOX, *J. Mater. Sci.* **10** (1975) 234.
5. I. VERPOEST and G.S. SPRINGER, *J. Reinf. Plastics & Compos.* **7** (1988) 23.
6. R.K. CLARK and W.B. LISAGOR, "Test Methods and Design Allowables for Fibrous Composites," ASTM STP734 (American Society for Testing and Materials, Philadelphia, PA, 1981) 34–53.
7. M.N. GHASEMI-NEJHAD and T.W. CHOU, *Composites* **21** (1990) 33.
8. T.A. BOGETTI, J.W. GILLESPIE and R.B. PIPES, *Comp. Sci. & Tech.* **32** (1988) 57.
9. M.R. PIGGOTT, in "Developments in Reinforced Plastics", edited by G. Pritchard (Elsevier Applied Science Publishers Ltd, London, 1984) p. 131.
10. R.M. VERETTE and J.D. LABOR, Air Force Technical Report AFFDLTR-76-142 (1977).
11. M.B. KASEN, R.E. SCHRAMM and D.J. READ, "Fatigue of Filamentary Composites". ASTM STP636 (American Society for Testing and Materials, Philadelphia, PA, 1977) p. 141.
12. J.M. WHITNEY, I.M. DANIEL and R.B. PIPES, "Experimental Mechanics of Fiber Reinforced Composite Materials." SESA Monograph no.4 (Prentice-Hall, Englewood Cliffs, NJ, 1982).
13. J.T. RYDER and E.D. BLACK, "Composite Materials: Testing and Design (Fourth Conference)" ASTM STP617 (American Society for Testing and Materials, Philadelphia, PA, 1977) p. 170.
14. R.B. LANTZ, *J. Comp. Mats.* **3** (1969) 642.
15. M.B. GRUBER, J.L. OVERBEEKE and T.W. CHOU *ibid* **10** (1982) 162.
16. D.H. WOOLSTENCROFT, A.R. CURTIS and R.I. HARESCEUGH, *Composites* **12** (1981) 275.
17. C.B. BUCKNALL and I.K. PARTRIDGE, *Polymer* **24** (1983) 639.
18. J.W. JOHNSON, Phil. Trans. R. Soc. **A294** (1980) 487.
19. I. GURNELL, Private communication (1991).
20. A. LOWE, see this issue.
21. Rolls Royce Process Specification MSRR9270 (1990).
22. M. FISCHER, Purchase Order EP3114842P Report no.1 Ciba Geigy, Marly (1989).
23. G.C. SIH and A.M. SKUDRA, "Handbook of Composites Volume 3." (Elsevier, London, 1985).
24. A. LOWE, unpublished work.
25. S.K. HA and G.C. SPRINGER in ICCM VI: Sixth International Conference on Composite Materials and ECCM 2: Second European Conference on Composite Materials, edited by F.L. Matthews, N.C.R. Buskell, J.M. Hodgekinson and J. Mortar, London **4** (Elsevier, London, 1987) pp. 422–428.

Received 23rd August 1994
and accepted 15th August 1995